

High-energy anomalies in covalent high- T_c cuprates with large Hubbard U_d on copper



O.S. Barišić^{a,*}, S. Barišić^b

^a Institute of Physics, Bijenička c. 46, HR-10000 Zagreb, Croatia

^b Department of Physics, Faculty of Science, University of Zagreb, Bijenička c. 32, HR-10000 Zagreb, Croatia

ARTICLE INFO

Available online 24 November 2014

Keywords:

Cuprates
Strong correlations
Emery model
Charge fluctuations
Diagrammatic theory
Slave fermions

ABSTRACT

A large U_d theory is constructed for the metallic state of high- T_c cuprates. The Emery three-band model, extended with O_x-O_y hopping t_{pp} , and with $U_d \rightarrow \infty$, is mapped on slave fermions. The Dyson time-dependent diagrammatic theory in terms of the Cu–O hopping t_{pd} , starting from the nondegenerate unperturbed ground state, is translationally and asymptotically locally gauge invariant. The small parameter of the theory is the average hole occupation of Cu sites n_d . The lowest order of the theory generates the single particle propagators of the hybridized pdp - and dpd -fermions with the exact covalent three band structure. The leading many-body effect is band narrowing, accompanied by Landau-like damping of the single particle propagation, due to incoherent local charge Cu–O fluctuations. The corresponding continuum is found below and above the Fermi level.

© 2014 Elsevier B.V. All rights reserved.

1. Introduction

The long standing question in high- T_c cuprates concerns the nature of low-frequency interactions which are responsible for superconductivity and other unusual properties of these materials. These effective interactions are related to the interplay between itinerancy and localization involving very large bare energy scales that characterize the electronic subsystem. In particular, it is well established that the Hubbard repulsion on copper sites U_d , which forbids the Cu double occupancy by holes, is the largest bare energy parameter. This implies that other bare parameters are strongly renormalized due to finite average hole occupation of Cu sites and, as such, observed in experiments. Accordingly, we have developed a strong-coupling diagrammatic perturbation formalism which starts from a hybridized metallic copper–oxygen state perturbed by forbidding the simultaneous double occupation on coppers [1]. Technically, this is achieved here through slave-fermion (spinful boson) formulation which avoids the usual but undesirable mean-field approximation.

Here, the physical expansion parameter turns out to be the time and space averaged average hole concentration on copper. In the absence of the mean field, the slave-particle propagators remain local (dispersionless), which introduces immediately (in low order) a distinction between local and itinerant single electron

states. In our approach, the double occupied copper states at high energies are at average empty and remain temporarily and spatially unresolved. Apparently, this is a reasonable tradeoff when U_d is large, i.e., in the charge transfer limit relevant for cuprates, $\Delta_{pd} < U_d$, with $\Delta_{pd} = \varepsilon_p - \varepsilon_d$, denoting the energy difference between the single occupied oxygen and copper sites. Referring to the LDA and similar results [2], the double occupied oxygen configuration is associated [3] with the energy $2\varepsilon_p$, i.e., U_p is considered as relatively small. This set of parameters was supplemented with the Cu–O hybridization t_{pd} and often called the Emery model [3] extended later [4,5] to include the O–O hopping t_{pp} .

The model is completed by fixing the total number of holes as $1 + x$ per CuO_2 unit cell, where x is the number of doped charge carriers (holes), assuming that $x \leq 1$. The average single particle occupations of the Cu and $O_{x,y}$ sites n_d and n_p are then linked by the sum rule $n_d + 2n_p = 1 + x$, i.e. $n_d - 2n_p$ or n_d itself is the “primary order parameter” of cuprates understood as Cu– O_2 charge transfer (CT) salts.

The aim of the current work is to exhibit key elements of our diagrammatic treatment of the strong-coupling limit in terms of slave particles and to explore low-order analytical expressions for single-particle propagators, explaining their limiting behaviors. Low-order calculations illustrate how the perturbation theory actually works and predict a window of (the “Fermi liquid”) coherency in the single particle spectrum around the Fermi level. That is, in addition to the metallic behavior [6,7] in the wide energy

* Corresponding author. Fax: + 385 1 469 88 89
E-mail address: obarisic@ifs.hr (O.S. Barišić).

window around the Fermi level, incoherent dispersionless continua are obtained on the retarded and advanced sides of the single hole spectra. The continua describe the effect on the test hole of the incoherent localized Cu–O charge transfer [8] fluctuations, precursors to the Mott localization. The advanced part is observed in ARPES measurements. A recent study based on the careful analysis of many ARPES experiments anticipates such type of the coherency window [9,10]. However, while the latter conclusion is based on partially phenomenological construction of the electron self-energy, in our case such behavior is obtained directly from the large U_d perturbation theory for the extended Emery model.

2. Slave fermion approach

It is well known that the $U_d = \infty$ Hamiltonian can be mapped on the slave particle Hamiltonian [12–14]. The empty hole d^{10} state on Cu at the position \vec{R} is denoted by $f_{\vec{R}}^{\dagger}|\bar{0}\rangle$ and the single occupied state d^9 with spin σ by $b_{\vec{R}\sigma}^{\dagger}|\bar{0}\rangle$, where $|\bar{0}\rangle$ is the auxiliary vacuum on Cu. In the so spanned three-state space (double occupied hole state d^8 with energy $2\varepsilon_d + U_d$ is omitted), the number operators of the slave particles satisfy $Q_{\vec{R}} = n_{f\vec{R}} + \sum_{\sigma} n_{b\vec{R}\sigma} = 1$. The physical fermion $d_{\vec{R}\sigma}^{\dagger}$ projected on the d^9 , d^{10} subspace is represented by the operator $d_{\vec{R}\sigma}^{\dagger} \rightarrow b_{\vec{R}\sigma}^{\dagger} f_{\vec{R}}$. The corresponding number operators satisfy $n_{\vec{R}\sigma}^{\dagger} = n_{b\vec{R}\sigma}^{\dagger}$, usually called the “Luttinger sum rule”. $b_{\vec{R}\sigma}^{\dagger}$ and $f_{\vec{R}}$ can be taken respectively as bosons and spinless fermions (“slave fermion representation”) in order to satisfy the anticommutation rules projected on the d^9 , d^{10} subspace for each Cu site, as well as the commutation rules between this site and other sites of the crystal.

In terms of these slave particles and p -fermions the Emery Hamiltonian in the $U_d = \infty$ limit is given by

$$H_0 = \varepsilon_b \sum_{\vec{k}, \sigma} b_{\vec{k}, \sigma}^{\dagger} b_{\vec{k}, \sigma} + \varepsilon_f \sum_{\vec{k}} f_{\vec{k}}^{\dagger} f_{\vec{k}} + \sum_{i, \vec{k}, \sigma} \varepsilon_{pk}^{(i)} p_{\vec{k}, \sigma}^{(i)\dagger} p_{\vec{k}, \sigma}^{(i)} \quad (1)$$

$$H_I = \frac{it_{pd}}{\sqrt{N}} \sum_{j, \sigma, \vec{k}, \vec{q}} \alpha^{(j)}(\vec{k}) b_{\vec{k} + \vec{q}, \sigma}^{\dagger} f_{\vec{q}} p_{\vec{k}, \sigma}^{(j)} + \text{h. c.} \quad (2)$$

$$\alpha^{(j)}(\vec{k}) = \sqrt{2} \left(\sin \frac{k_x}{2} \pm \text{sgn}(k_x k_y) \sin \frac{k_y}{2} \right). \quad (3)$$

It is locally $U(1)$ gauge invariant and commutes with the operator $Q_{\vec{R}}$. The O site energy ε_p and the O–O hopping t_{pp} are included in H_0 . On the other hand, H_I is proportional to Cu–O hopping t_{pd} equal along both axes, which renders the Hamiltonian $D4$ symmetric. The usual sign convention is $t_{pp} < 0$, $t_{pd} > 0$. In the hole picture, cuprates are characterized by a positive charge transfer energy $\Delta_{pd} > 0$.

H_0 is defined by bare site energies ε_b and ε_f of bosons (spinons) and chargons (spinless fermions) under restriction $\varepsilon_b - \varepsilon_f = \varepsilon_d$ consistently with the composite representation $d_{\vec{R}\sigma}^{\dagger} \rightarrow b_{\vec{R}\sigma}^{\dagger} f_{\vec{R}}$ of the truncated Fermi operator $d_{\vec{R}\sigma}^{\dagger}$. We notice for later convenience that the site energies ε_b and ε_f can be taken to include the slave particle chemical potentials conjugated respectively to the mean number of fermions n_f and bosons n_b . In this respect, $(\varepsilon_f - \varepsilon_b)/2$ is the “external field” conjugated to $n_f - n_b$ and $(\varepsilon_f + \varepsilon_b)/2$ to the $U(1)$ invariant charge $n_f + n_b = Q = 1$.

3. Diagrammatic perturbation theory

Our intention here is to treat the model (2) by using the time-ordered diagrammatic perturbation theory in terms of the Cu–O “coupling” t_{pd} . Being concerned with metallic properties of cuprates a translationally and $U(1)$ invariant paramagnetic unperturbed ground state is of special interest. The only eigenstate of H_0 with such properties puts all available charge $1+x$ on oxygens and localizes one slave fermion $f_{\vec{R}\sigma}^{\dagger}$ on each Cu-site. Expressed in the reciprocal space, such slave fermion state is strictly equivalent to the completely filled dispersionless band of spinless fermions. In this way, one gets the diagrammatic perturbation theory amenable to direct application of Wick’s time-ordering theorem in the reciprocal space. Correlation functions in the reciprocal space exhibit the localized phenomena as dispersionless features, while itinerant ones are characterized by associated dispersions. However, as far as the $U(1)$ invariance is concerned, the diagrammatic perturbation theory obeys it only asymptotically, in the sense that the hypothetical summation of all diagrams is required.

The elementary bricks which build the time-dependent perturbation theory according to Wick’s theorem are the free-particle propagators. Defining, as usual, $B(\vec{k}, t) = -i\langle T b_{\vec{k}}^{\dagger} b_{\vec{k}}(t) \rangle$, $F(\vec{k}, t) = -i\langle T f_{\vec{k}}^{\dagger} f_{\vec{k}}(t) \rangle$, we find that the free propagators of the b - and f -particles are dispersionless,

$$B^{(0)} = \frac{1}{\omega - \varepsilon_b + i\eta}, \quad F^{(0)} = \frac{1}{\omega - \varepsilon_f - i\eta}. \quad (4)$$

Through $+i\eta$ $B^{(0)}$ describes the intermittent creation of the b -particle, while, the spinless fermions can only be annihilated.

The d -particle propagator is mapped on

$$D_{\vec{k}}(t) = -(i/N) \langle T \sum_q f_q^{\dagger} b_{\vec{k}+q} f_q(t) b_{\vec{k}+q}^{\dagger}(t) \rangle. \quad (5)$$

$D_{\vec{k}}^{(0)}$ is thus also dispersionless. With $\varepsilon_b - \varepsilon_f = \varepsilon_d$, one obtains $D_{\vec{k}}^{(0)} = (\omega - \varepsilon_d + i\eta)^{-1}$. Regarding oxygen sites, according to their Fermi distribution $f_k^{(i)}$, the free propagators of $1+x$ p -particles contain both $+i\eta$ and $-i\eta$ components $G_p^{(i)>}(\vec{k}, \omega)$ and $G_p^{(i)<}(\vec{k}, \omega)$, associated with the $i = l, \bar{l}$ bands. The corresponding chemical potential is hereafter denoted by $\mu^{(0)}$. With $x < 1$, only the states in the l -band are occupied.

With free propagators defined, one may now derive general expressions for the r -th order time-dependent perturbation theory. According to the mapping of the d -hole on the slave particle-hole pair, $D_{\vec{k}}^{(r)}(\omega)$ is given by the (generalized) Bethe–Salpeter equation,

$$D_{\vec{k}}^{(r)}(\omega) = \Sigma_{\vec{k}}^{(r-1)}(\omega) + \Sigma_{\vec{k}}^{(r-1)}(\omega) \Gamma_{\vec{k}}^{(r)}(\omega) \Sigma_{\vec{k}}^{(r-1)}(\omega). \quad (6)$$

Here, $\Sigma_{\vec{k}}^{(r)}$ is the quantity irreducible with respect to cutting the p -lines and $\Gamma_{\vec{k}}^{(r)}(\omega)$ is the renormalized four-leg vertex (“translation propagator” [15]), given iteratively by the Dyson equation,

$$\Gamma_{\vec{k}}^{(r)}(\omega) = \Gamma_{\vec{k}}^{(0)}(\omega) + \Gamma_{\vec{k}}^{(0)}(\omega) \Sigma_{\vec{k}}^{(r-1)}(\omega) \Gamma_{\vec{k}}^{(r)}(\omega), \quad (7)$$

in terms of the bare four-leg vertex $\Gamma_{\vec{k}}^{(0)}(\omega)$, given by

$$t_{pd}^{-2} \Gamma_{\vec{k}}^{(0)}(\omega) = \alpha_{\vec{k}}^{(l)2} G_p^{(l)<}(\vec{k}, \omega) + \sum_{j=l, \bar{l}} \alpha_{\vec{k}}^{(j)2} G_p^{(j)>}(\vec{k}, \omega), \quad (8)$$

with $\alpha_{\vec{k}}^{(j)}$ given by Eq. (3). Eq. (8) generalizes the bare four-leg vertex used previously [17] for $t_{pp} = 0$.

3.1. $r=1$ band structure

The lowest order $\Sigma_k^{(0)}$ is simply equal to $D^{(0)}$. In other words, $D^{(0)}$ is not only the elementary d -particle propagator but also the lowest order “local” irreducible self-energy for $\Gamma_k^{(1)}$. The $r=1$ procedure separates out the \vec{k} -independent d -propagator $D^{(0)}$ in the leading pdp -particle self-energy on associating in Eq. (8) the \vec{k} -dependence of triangular vertices with the appropriate \vec{k} -dependent weighting within the free translation propagator $t_{pd}^{-2}\Gamma_k^{(0)}$.

$t_{pd}^{-2}\Gamma_k^{(1)}$ and $D_k^{(1)}$ in the Dyson form exhibit coherent poles belonging to three bands $\omega_k^{(j)}$ denoted by $j = L, I, U$. The poles $\omega_k^{(j)}$ in $t_{pd}^{-2}\Gamma_k^{(1)}$ are associated with the residuals (spectral weights) $z_k^{(j)}$. These spectral weights can be expressed entirely in terms of the three $\omega_k^{(j)}$. In particular, one may express first the spectral weight $z_k^{(L)}$ of the hole prepared on the Cu-site which propagates in the L -band appearing in the $D_k^{(1)}$ propagator according to Eq. (6). For example, for the lowest band L , one obtains

$$z_k^{(L)} = \frac{(\omega_k^{(L)} - \varepsilon_{pk}^{(I)}) (\omega_k^{(L)} - \varepsilon_{pk}^{(U)})}{(\omega_k^{(L)} - \omega_k^{(I)}) (\omega_k^{(L)} - \omega_k^{(U)})}, \quad (9)$$

and similarly for other two bands. In the next step, somewhat counter-intuitively, one gets that $z_k^{(L)}$ and $z_k^{(Ld)}$ are proportional,

$$t_{pd}^2 z_k^{(L)} = z_k^{(Ld)} \left(\varepsilon_d - \omega_k^{(L)} \right)^2. \quad (10)$$

The spectral weight $z_k^{(Lp)}$ corresponding to the p -propagator of the hole created symmetrically on two oxygen sites is given by $z_k^{(Lp)} = 1 - z_k^{(Ld)}$ [15].

The chemical potential $\mu^{(1)}$ of the p -fermions is next defined as the energy which positions in the upper and lower ω -plane poles all common to the three kinds of propagators. This step fixes the pole positions, consistently with the fermionic nature of the $b^i f$ pairs. In contrast to $\mu^{(0)}$, which defines the average number of p -fermions on the O-sites, $\mu^{(1)}$ can thus be conjugated to the average number of particles in the coherent states on O and Cu sites. In other words, $\mu^{(1)}(\Delta_{pd}, t_{pd}, t_{pp}, x)$ can be determined through the average charge conservation rule $n_d^{(1)} + 2n_b^{(1)} = 1 + x$, bearing in mind that $n_b^{(1)}$ and $n_d^{(1)}$ are defined by Eqs. (6) and (7) as functions of the band parameters and $\mu^{(1)}$. Thus, as a result of our strong-coupling perturbation theory, the whole $r=1$ procedure described above amounts to the redistribution of the spectral weights and the Fermi occupation factors $f_k^{(i)}$ (with accompanying $\pm i\eta$'s) from two oxygen bands $i = I, \tilde{I}$ and the empty d -state into the three coherently hybridized Hartree-Fock (HF) bands $\omega_k^{(j)}$, $j = L, I, U$ of covalent [16], itinerant *noninteracting* states.

3.2. $r=2$ corrections and hole correlations

We turn next to the properties of the slave-particle propagators $B^{(1)}(\omega)$ and $F^{(1)}(\omega)$. In particular, these propagators will be used to construct the next order $r=2$ iteration of Eqs. (6) and (7), describing *correlations* between physical particles. The bubbles which appear in Fig. 1 are the lowest order irreducible Dyson self-energies for $B^{(1)}(\omega)$ and $F^{(1)}(\omega)$. They both involve summation over the occupied states in the l -band as indicated in Fig. 1 by the p -propagator going (only) backwards in time.

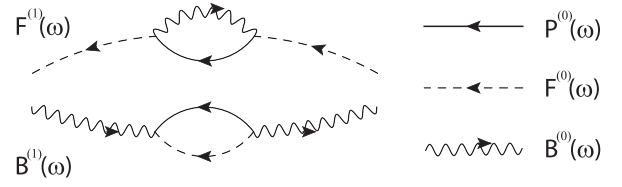


Fig. 1. Lowest order renormalization for the slave particle propagators $B(\omega)$ and $F(\omega)$, with arrows of time shown. The free propagators for the b and the f slave particle are denoted by $B^{(0)}(\omega)$ and $F^{(0)}(\omega)$, respectively, while $P^{(0)}(\omega)$ is the p -propagator.

The b -bubble is \vec{k} -independent (local), given by

$$\beta^{(1)}(\omega) = \frac{t_{pd}^2}{N} \sum_{\vec{k}} \frac{z_k^{(L)} f_k^{(L)}}{-\omega + \omega_k^{(L)} + \varepsilon_f + 2i\eta}, \quad (11)$$

where $z_k^{(L)}$ are the residues of the propagators $t_{pd}^{-2}\Gamma_k^{(1)}$ given by Eqs. (9) and (10). The spinless fermion self-energy $\phi^{(1)}(\omega)$ has a structure similar to Eq. (11),

$$\phi^{(1)}(\omega) = \frac{2t_{pd}^2}{N} \sum_{\vec{k}} \frac{z_k^{(L)} f_k^{(L)}}{\omega + \omega_k^{(L)} - \varepsilon_b + 2i\eta}. \quad (12)$$

Dealing with only a partial summation of the exact perturbative series, the average $U(1)$ invariance of spinon and chargin average numbers $n_b^{(r)}$, $n_f^{(r)}$,

$$n_b^{(r)} = n_d^{(r)}, \quad n_f^{(r)} + n_b^{(r)} = 1, \quad (13)$$

is not achieved in general. However, this can be avoided by treating $\varepsilon_b^{(r)}$ and $\varepsilon_f^{(r)}$ as chemical potentials according to a scheme given by

$$B^{(r)}(\omega) = \frac{1}{\omega - \varepsilon_b^{(r)} + i\eta - t_{pd}^2 \beta^{(r-1)}(\omega)}, \quad (14)$$

$$F^{(r)}(\omega) = \frac{1}{\omega - \varepsilon_f^{(r)} - i\eta - t_{pd}^2 \phi^{(r-1)}(\omega)}, \quad (15)$$

where $\varepsilon_b^{(r)}$ and $\varepsilon_f^{(r)}$ are fixed to obey Eq. (13). That is, in Eqs. (14) and (15) the slave chemical potential pair, $\varepsilon_b^{(r)}$ and $\varepsilon_f^{(r)}$, is uniquely determined by the two physical conditions (13) for $n_b^{(r)}$ and $n_f^{(r)}$, with a particularly convenient property of keeping the average $U(1)$ symmetry iteratively, step by step in r . Since the exact perturbation theory is locally gauge invariant, a reasonable conjecture is that the iterative sequence $\varepsilon_b^{(r)}$ and $\varepsilon_f^{(r)}$ tends to $\varepsilon_b^{(0)}$ and $\varepsilon_f^{(0)}$ of the original Hamiltonian as r increases.

The spectral weight associated to the $r=1$ boson and fermion propagators is shown in Fig. 2 for band parameters $\Delta_{pd}/t_{pd} = 3/2$, $t_{pp} = -t_{pd}$ and $x=0$. As it may be observed from Fig. 2, $B_\lambda^{(1)}(\omega)$ can be written in terms of one pole in the negative ω -half-plane and a set of poles in the positive ω -half-plane, $B^{(1)} = B^{(1)>} + B^{(1)<}$, and $f \leftrightarrow b$ symmetrically for $F^{(1)} = F^{(1)<} + F^{(1)>}$ (the superscripts $<$ and $>$ denote arrows of time).

Once $B^{(1)}(\omega)$ and $F^{(1)}(\omega)$ have been determined, they can be used to calculate $\Sigma^{(1)} \sim (B^{(1)} * F^{(1)})$ in Eqs. (6) and (7), i.e. to advance the iteration one step further to find the propagators $D_k^{(2)}$ and $\Gamma_k^{(2)}$ of the physical particles. In particular, the relevant contributions to the convolution $\Sigma^{(1)} \sim (B^{(1)} * F^{(1)})$ come from the poles on the opposite sides of the ω -axis,

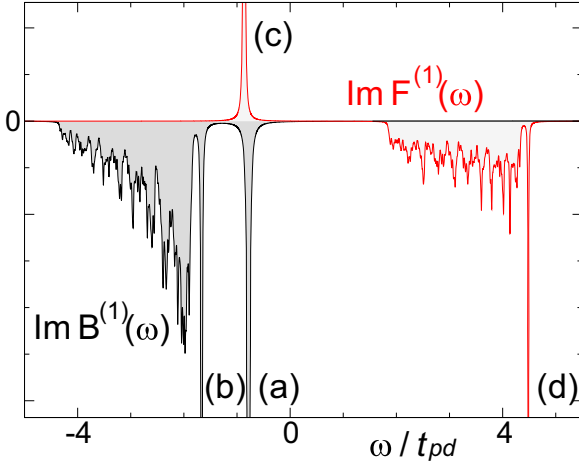


Fig. 2. The $r=1$ boson and fermion propagators $\text{Im } B^{(1)}(\omega)$ and $\text{Im } F^{(1)}(\omega)$ (in arbitrary unit) for $\chi=0$ and for band parameters $\Delta_{pd}/t_{pd}=3/2$, $t_{pp}=-t_{pd}$, i.e. $n_d^{(1)}=0.4$. (a) Denotes the advancing boson pole $B^{(1)>}$, (b) the receding pole $B^{(1)<}$ detached from the dense set of receding poles and analogously (c) and (d) respectively $F^{(1)<}$ and $F^{(1)>}$ for spinless fermion. In the numerical calculation here the Brillouin zone is sampled by 1024 k points.

$$\begin{aligned}\Sigma^{(1)} &= \Sigma^{(1)>} + \Sigma^{(1)<} \\ &= \frac{-i}{2\pi} (B^{(1)>} * F^{(1)<} + B^{(1)<} * F^{(1)>}).\end{aligned}\quad (16)$$

$\Sigma^{(1)>}$ is “local” in the direct space (dispersionless),

$$\Sigma^{(1)>} = \frac{(1 + n_b^{(1)}/2)n_f^{(1)}}{\omega - \varepsilon_d^{(1)} + 2i\eta}\quad (17)$$

$$\Sigma^{(1)<} = \frac{t_{pd}^4}{N^2} \sum_{\vec{k}, \vec{k}'} \frac{f_{\vec{k}, \vec{k}'}^{(L)} f_{\vec{k}, \vec{k}'}^{(L)} A_{\vec{k}, \vec{k}'}^{\rightarrow, \rightarrow}}{\omega - \tilde{\omega}_{b\vec{k}}^{(L)} - \tilde{\omega}_{f\vec{k}'}^{(L)} + \varepsilon_d - 4i\eta}.\quad (18)$$

The spectral weight of the leading pole $\Sigma^{(1)>}$ of Eq. (17) describes the average reduction in the availability of the given Cu-site for the free propagation of the additional hole due to incoherent Cu–O fluctuations of the permanent holes. The quantity $n_b^{(1)}n_f^{(1)}/2$ can thus be understood as the average projector which removes the d-states from the coherent propagation. The reduction of $\Sigma^{(1)>}$ is nominally quadratic in t_{pd} since such are the generic contributions to $n_b^{(1)}$ and $1 - n_f^{(1)}$.

In contrast to $\Sigma^{(1)>}$, the receding $(-i\eta)$ continuum of $\Sigma^{(1)<}$ describes the dynamic local disorder due to Cu–O charge transfer fluctuations. In the limit $N \rightarrow \infty$, $\text{Im } \Sigma^{(1)<}$ for $n_d^{(1)}$ small is a step-like function finite in the range $2\mu^{(1)} - \varepsilon_d > \omega > 2\omega_M - \varepsilon_d$, where ω_M is the minimum of the conducting L band. t_{pd}^4 in Eq. (18) for $\Sigma^{(1)<}$ is exhibited in order to stress that the generic term in the t_{pd} expansion of $\Sigma^{(1)<}$ is nominally quartic in t_{pd} which results in the total spectral weight associated with the set of dense poles (continuum) equal to $(n_d^{(1)})^2$. Apparently, already this result goes well beyond the HF or many HF-inspired theories.

3.2.1. $r=2$ pdp propagator

The translation propagator $t_{pd}^{-2}\Gamma_{\vec{k}}^{(2)}$ is determined by $\Sigma^{(1)}$ according to Eq. (7). Thus it also undergoes a modification of the coherent spectral weight and exhibits the effects of dynamical Cu–O disorder. Let us thus consider this propagator in some detail. In the first step we keep $\Sigma^{(1)>}$ but omit $\Sigma^{(1)<}$. Eq. (7) for $\Gamma_{\vec{k}}^{(2)}$ combined with $\Sigma^{(1)>}$ gives then the band narrowing and the relatively small renormalization of the CT gap, while ε_p , as well as t_{pp} , remain

unaffected,

$$t_{pd}^2 \rightarrow t_{pd}^{(1)2} = t_{pd}^2 \left(1 + \frac{1}{2}n_b^{(1)}n_f^{(1)}\right),$$

$$\Delta_{pd} \rightarrow \Delta_{pd}^{(1)} = \varepsilon_p - \varepsilon_d^{(1)} = \Delta_{pd} + \beta_\lambda^{(1)}(\omega = \varepsilon_d^{(1)} + \lambda),\quad (19)$$

For $n_d^{(1)}$ small one obtains $t_{pd}^2 \rightarrow t_{pd}^2(1 - n_d^{(1)}/2)$. Such renormalization is about half of that predicted [11,18] by the mean field slave boson theory. Concomitantly, $\Delta_{pd}^{(1)}$ is somewhat decreased with respect to Δ_{pd} similarly to the mean field slave boson theory.

Next we include $\Sigma^{(1)<}$ perturbatively and get

$$\text{Im } \Gamma_{\vec{k}}^{(2)}(\omega) \approx \sum_j \frac{t_{pd}^2(\eta_S + z_{j,k}^{(2)} t_{pd}^2 \text{Im } \Sigma^{(1)<})}{(\omega - \omega_{j,k}^{(2)})^2 + (\eta_S + z_{j,k}^{(2)} t_{pd}^2 \text{Im } \Sigma^{(1)<})^2}.\quad (20)$$

where $\eta_S = \eta \text{sgn}(\mu^{(2)} - \omega_{j,k}^{(2)})$ and $\mu^{(2)}$ remains to be determined.

For simplicity, $z_{j,k}^{(2)} \text{Re } \Sigma^{(1)<}$ is omitted above, being related to the presumably small (logarithmic) corrections. The poles $\omega_{j,k}^{(2)}$ are thus given by the coherent band narrowing of Eq. (19) and the residues $z_{j,k}^{(2)}$, which correspond to $\omega_{j,k}^{(2)}$, are obtained from Eq. (9) upgraded to $r=2$.

$\text{Im } \Sigma^{(1)<}$ generates contributions to $t_{pd}^{-2}\Gamma_{\vec{k}}^{(2)}$ beyond the coherent band narrowing. Apparently, the effect of $\text{Im } \Sigma^{(1)<}$ should be interpreted as inelastic Landau-like damping of the coherent pdp propagation by incoherent $b^{\dagger}f$ pairs, i.e., by local incoherent Cu–O charge transfer fluctuations. As well known, the Landau damping corresponds to energy, rather than to momentum relaxation. The corresponding pseudo-particle width is then conveniently approximated by a remarkably transparent expression

$$\frac{2\pi}{\tau_{\vec{k}}^{(2)}} = t_{pd}^2 z_{L,\vec{k}}^{(2)} \text{Im } \Sigma^{(1)<}(\omega_{L,\vec{k}}^{(2)}).\quad (21)$$

$\text{Im } \Sigma^{(1)<}$ is taken here at $\omega = \omega_{L,\vec{k}}^{(2)}$, characterizing the broadening of the Dirac functions into the Lorentzians. On the other hand, according to Eq. (9), the weight of the affected d-states is measured by $z_{L,\vec{k}}^{(2)}$.

Turning now to the sum rules we note that the Lorentzian $\tau_{\vec{k}}^{(2)}$ of Eq. (21) does not affect the renormalized HF contribution $n_p^{(2HF)}$ to $n_p^{(2)}$. For a given chemical potential $\mu^{(2)}$ we thus have

$$n_p^{(2)} \approx n_p^{(2HF)} + n_p^{(2inc)}.\quad (22)$$

where $n_p^{(2inc)}$ is the correction to the Lorentzian approximation. This term, which includes the variation of $\text{Im } \Sigma^{(1)<}$ far from the band, can be neglected on the simplest level.

3.2.2. $r=2$ dpd -propagator, sum rules and the chemical potential

In contrast to the translation and pdp propagators, the $r=2$ dpd -propagator given by Bethe–Salpeter Eq. (6) entirely reveals the local Cu–O fluctuations. Beside the coherent and Landau damped propagation, its first term exhibits $\text{Im } \Sigma^{(1)<}$ of Eq. (18) which is finite not only above but also below the bottom of the $L^{(2)}$ -band, all over the Brillouin zone in the frequency range $2\omega_M - \varepsilon_d < \omega < 2\mu^{(1)} - \varepsilon_d$, where the coherent hybridization is absent.

Concerning first the coherent dpd propagation, Eq. (6) shows that some of the coherent spectral weight on copper is removed, i.e. the latter is depleted to $z_{j,k}^{(2d)} = (1 + \frac{1}{2}n_b^{(1)})n_f^{(1)}z_{j,k}^{(2dHF)}$. Here

$z_{j,\vec{k}}^{(2dHF)}$ is the $r=2$ renormalized HF spectral weight defined by the self-energy $\Sigma^{(1)>}$ of Eq. (17) divided by $(1 + n_b^{(1)}/2)n_f^{(1)}$ and given by the upgraded Eq. (9). Due to such depletion of the coherent spectral weight $z_j^{(2d)}$ the first, coherent term in $n_d^{(2)}$ of Eq. (23) is somewhat smaller than $n_d^{(2HF)}$ calculated from the renormalized HF bands for a given chemical potential $\mu^{(2)}$. E.g. for $n_d^{(1)} \approx n_b^{(1)} \approx 1 - n_f^{(1)}$ small Eq. (23) can be used, on linearizing in terms of $n_d^{(2HF)} - n_d^{(1)}$, to write $n_d^{(2coh)} \approx n_d^{(2HF)} - (n_d^{(1)})^2/2$. In this sense it can be said that the $r=2$ HF band plays an auxiliary role.

In contrast to that, the propagation in the incoherent frequency range is dominated by the first term $\text{Im} \Sigma^{(1)<}$ in Eq. (6), explicitly related to the local Cu–O fluctuations. The locality of this term is the precursor of the Mott localization within the CuO_2 unit cell, which occurs for other choices of x and/or band parameters. In the simplest approximation $n_d^{(2inc)}$ is obtained by integrating $\text{Im} \Sigma^{(1)<}$ of Eq. (18), with the particularly simple result, namely $n_d^{(2inc)} = n_b^{(1)}(1 - n_f^{(1)})$ which reduces to $n_d^{(2inc)} \approx (n_d^{(1)})^2$ for $n_d^{(1)}$ small.

The coherent $\Sigma^{(1)>}$ and incoherent $\Sigma^{(1)<}$ components contribute then essentially additively to average occupations of the Cu sites, i.e. $n_d^{(2)} \approx n_d^{(2coh)} + n_d^{(2inc)}$. We have therefore

$$n_d^{(2)} \approx \left(1 + \frac{1}{2}n_b^{(1)}\right)n_f^{(1)}n_d^{(2HF)} + n_d^{(2inc)}. \quad (23)$$

Putting these two contributions to $n_d^{(2)}$ together on keeping in mind that $n_d^{(2HF)}$ depends, as well as $n_b^{(2HF)}$, on the chemical potential $\mu^{(2)}$ one finds this latter from the sum rule $n_d^{(2)} + 2n_b^{(2)} = 1 + x$. This is well illustrated for $n_d^{(1)}$ small on writing

$$\begin{aligned} n_d^{(2HF)} + 2n_b^{(2HF)} &\approx 1 + x_{\text{eff}}^{(2)}, x_{\text{eff}}^{(2)} \\ &= x + \frac{1}{2}n_d^{(1)2} - n_d^{(2inc)} \\ &= x - \frac{1}{2}(n_d^{(1)})^2. \end{aligned} \quad (24)$$

$\mu^{(2)}$ corresponds thus to the HF chemical potential for the effective doping $1 + x_{\text{eff}}^{(2)}$ reduced with respect to $1 + x$. Such $1 + x_{\text{eff}}^{(2)}$ is put into the $L^{(2)}$ -band renormalized according to Eq. (19). The conventional Luttinger sum rule for the band states (to be distinguished from the Luttinger sum rule $n_d = n_b$) is broken. The reason is that the occupied localized disorder states on copper carry more spectral weight than transferred on copper from the occupied itinerant states. The departure from the conventional Luttinger sum rule is however small for $n_d^{(1)}$ small. The whole procedure results in $n_d^{(2)} > n_d^{(1)}$, i.e., the local Cu–O fluctuations increase the average copper occupation with respect to its HF values $n_d^{(1)}$ and $n_d^{(2HF)}$.

It can be finally emphasized that the $r=2$ results appear above as an expansion in terms of $n_d^{(1)}$. The present theory, where $d=2$ explicitly, is thus not an expansion in the number of dimensions or in large orbital and/or spin degeneracy. Even the $N \rightarrow \infty$ limit is unessential here, used only for the analytic calculation of the coefficients $n_b^{(1)}$, $n_f^{(1)}$, $\bar{\epsilon}_d$, $A_{\vec{k},\vec{k}'}$, $\bar{\omega}_{\vec{k}}^{(L)}$ in Eqs. (17) and (18).

3.3. $r=3$ contributions

The $r=2$ theory described above in some detail illustrates how to analytically derive important features of the single-hole states in presence of large U_d on copper. Next we turn to the $r=3$ step of the diagrammatic expansion. If the four-leg effective kinematical

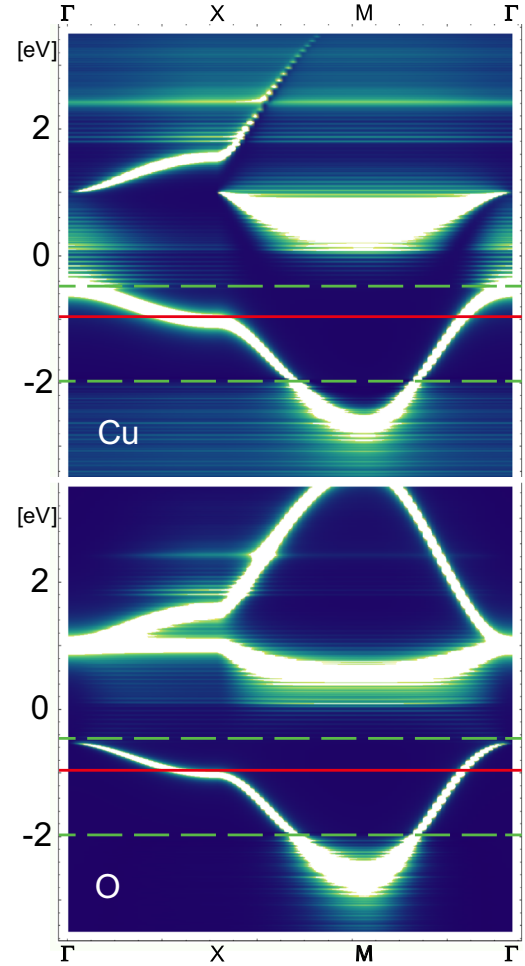


Fig. 3. The $r=3$ single-hole spectral weight projected on the Cu and the O site, with $\Delta_{pd} = 1$ eV, $t_{pd} = -t_{pp} = 0.7$ eV, $x=0.2$, shown along high symmetry lines of the Brillouin zone $\Gamma - X - M - \Gamma$. The full line denotes the Fermi level E_F . Notice the formation of the coherency window between the two dashed lines.

interactions [19], quartic in t_{pd} , are neglected, which is justified well away from the Fermi level, the $r=2$ and $r=3$ theories are similar in principle. Essentially, what $r=2$ theory does to the retarded hole continua, $r=3$ theory does to the advanced continua. Some preliminary $r=3$ numerical results are shown in Fig. 3.

The results for the $r=3$ single-hole spectral weight projected on copper and oxygen sites, as functions of \vec{k} and ω , are shown in Fig. 3, for a set of bare parameters that mimic typical behaviors in cuprates, $\Delta_{pd} = 1$ eV, $t_{pd} = -t_{pp} = 0.7$ eV. Standard cuts through the Brillouin zone are considered, setting the doping in Fig. 3 to $x=0.2$. Few characteristic spectral behaviors are immediately observed. The first is the coherent conduction band that intersects the Fermi energy E_F , given by the red line. At elevated frequencies, denoted by the two dashed lines, this band enters broad continua, found on the retarded and the advanced side of the $r=3$ spectra, the latter observable in ARPES measurements. That is, the incoherent spectral weight above the Fermi energy in Fig. 3 is found approximately for frequencies $\omega - E_F \gtrsim 0.4$ eV, in very good agreement with ARPES experiments for various hole-doped cuprates. Evaluated depletion of the coherent spectral weight also agrees with that deduced phenomenologically from conduction measurements [20]. Most of other properties examined within the present scheme are consistent with only three single particle parameters Δ_{pd} , t_{pd} , t_{pp} used here, as will be discussed elsewhere.

The kind of itinerant-localized, coherent-incoherent dichotomy in single-hole spectra, seen in Fig. 3, is usually referred to, in the context of ARPES measurements, as the high-energy anomaly (HEA) [21]. For electron doped cuprates, $x < 0$, the HEA is reported at approximately twice as large frequency as for the hole doped cuprates, 0.8 vs. 0.4 eV [22–27]. This is exactly what one obtains within the $r=3$ calculations, by summing the non-crossing diagrams. Such result is easy to visualize. As x increases and the Fermi level approaches ε_d , the local charge Cu–O fluctuations spread out, narrowing the window of coherency around the Fermi level, obtained in Fig. 3.

Besides the window of coherency around the Fermi level (where incoherencies might appear due to kinematical interactions), the diagrammatic calculations predict additional, doping dependent effects. In particular, regarding the coherent part of the spectrum, the band dispersions become weaker as x increases. The corresponding spectral weights get depleted in contrast to incoherent features which are enhanced. For example, one finds that the nodal velocity at the Fermi level decreases with increasing hole concentration x , clearly indicating a stronger quasi-particle renormalization. Increasing x means increasing mean occupation of copper sites, i.e., increasing strength of correlations. Such behaviors have been recently observed by ARPES measurements on electron and hole doped cuprates [10,28,29].

References

- [1] S. Barišić, O.S. Barišić, Physica B 404 (2009) 3;
S. Barišić, O.S. Barišić, J. Supercond. Nov. Magn. 25 (2012) 669;
G. Nikšić, O.S. Barišić, I. Kupčić, D.K. Sunko, S. Barišić, Physica B 407 (2012) 1831.
- [2] L.F. Mattheiss, Phys. Rev. Lett. 58 (1987) 1028.
- [3] V.J. Emery, Phys. Rev. Lett. 58 (1987) 2794.
- [4] P. Lederer, G. Montambaux, D. Poilblanc, J. Phys. 48 (1987) 1613.
- [5] J.H. Kim, K. Levin, A. Auerbach, Phys. Rev. B 39 (1989) 11633.
- [6] N. Barišić, et al., Proc. Natl. Acad. Sci. 110 (2013) 12235;
S.J. Mirzaei, et al., Proc. Natl. Acad. Sci. 110 (2013) 5774.
- [7] L.P. Gor'kov, Phys. Rev. B 88 (2013) 041104(R).
- [8] L.P. Gor'kov, A.V. Sokol, JETP Lett. 46 (1987) 420.
- [9] R. Comin, et al., Science 24 (2014) 390.
- [10] B. Moritz, et al., New J. Phys. 11 (2009) 093020.
- [11] G. Kotliar, A.E. Ruckenstein, Phys. Rev. Lett. 57 (1986) 1362.
- [12] S.E. Barnes, J. Phys. F 6 (1976) 1375.
- [13] A. Houghton, N. Read, H. Won, Phys. Rev. B 37 (1988) 3782.
- [14] P. Coleman, Phys. Rev. B 29 (1984) 3035.
- [15] Notice that $\Gamma_{\vec{r}}^{(p)}(\omega)$ propagator slightly differs from the conventional p -propagator, which defines the propagation of the hole created/annihilated on oxygen sites.
- [16] J. Friedel, J. Phys. Condens. Matter 1 (1989) 7757.
- [17] H. Nikšić, E. Tutiš, S. Barišić, Physica C 241 (1995) 247.
- [18] I. Mrkonjić, S. Barišić, Eur. Phys. J. B 34 (2003) 69;
I. Mrkonjić, S. Barišić, Eur. Phys. J. B 34 (2003) 441.
- [19] S. Barišić, O.S. Barišić, arXiv:1110.1947.
- [20] I. Kupčić, S. Barišić, Phys. Rev. B 75 (2007) 094508.
- [21] W. Meevasana, et al., Phys. Rev. B 75 (2007) 174506.
- [22] Z.-H. Pan, et al., cond-mat/0610442.
- [23] J. Graf, et al., Phys. Rev. Lett. 98 (2007) 067004.
- [24] D.S. Inosov, et al., Phys. Rev. Lett. 99 (2007) 237002.
- [25] W. Zhang, et al., Phys. Rev. Lett. 101 (2008) 017002.
- [26] M. Ikeda, T. Yoshida, A. Fujimori, M. Kubota, K. Ono, Y. Kaga, T. Sasagawa, H. Takagi, Phys. Rev. B 80 (2009) 184506.
- [27] F. Schmitt, et al., Phys. Rev. B 83 (2011) 239905.
- [28] X.J. Zhou, et al., Nature 423 (2003) 398.
- [29] M. Hashimoto, et al., Phys. Rev. B 77 (2008) 094516.